JOURNAL OF MATERIALS SCIENCE 27 (1992) 963–971

Stabilization of SnO_2 ultrafine particles by additives

C. XU, J. TAMAKI, N. MIURA, N. YAMAZOE
Department of Materials Science and Technology, Graduate School of Engineering Sciences, Kyushu University, Kasuga, Fukuoka 816, Japan

In order to stabilize ultrafine particles of SnO_2 which is essential to obtain high gas sensitivity, a systematic investigation was undertaken regarding the stabilizing effects of 5 at% impregnated foreign additives, consisting of oxides or polyoxy compounds of 31 metals and 3 non-metals. The data of specific surface area, SA, as well as SnO_2 crystallite size, D, evaluated from X-ray diffraction showed that the additives could be classified into several groups according to the effectiveness. The most effective group, consisting of P–Ba, Sm, Ba, P, Mo, W, Ca, Sr, Cr and In, could keep D less than 10 nm even after calcination at 900 °C, whereas pure SnO_2 underwent grain growth to have D of 13 and 27 nm at 600 and 900 °C, respectively. Electron microscopy revealed that neck sizes, X, between crystallites were fairly proportional to D ($X/D = 0.80$). A simple analysis of SA and D data based on a monosized sphere model suggested that each crystallite was coordinated with 3–4.5 neighbours through the necks. The existing state and stabilizing mechanism of additives are discussed in conjunction with the electrical resistance of porously sintered elements.

1. Introduction

SnO_2 has long been exploited in semiconductor gas sensors. To meet ever increasing needs for new sensors, many attempts have been made to improve sensing properties of SnO_2-based gas sensors. Recently, we have found that the gas sensitivity of an SnO_2 sensor can be promoted greatly by using ultrafine particles of SnO_2, especially at a size around 5 nm [1]. The crystallite size of pure SnO_2, however, increases tremendously when subjected to heat treatments at high temperature, no matter how they are prepared [2–5]. It is not possible to keep the particles in the ultrafine state during the sintering process of sensor fabrication currently in practice. Thus an effective way to stabilize SnO_2 particles at high temperature is eagerly awaited. In a previous article, we reported preliminarily results showing that some additives were quite effective for this purpose [6]. The present paper aims to examine in more detail the stabilizing effect of a wide variety of oxides or polyoxy compounds of metals or non-metals. Parameters characterizing the ultrafine state of SnO_2 (specific surface area and the crystallite size of SnO_2) were investigated after heat treatment (calcination) at 600–900 °C. In order to elucidate the stabilizing effects of various additives, electron microscopic observation was also carried out to reveal the microstructure of the polycrystalline state. The electrical resistance of impregnated samples as well as its variation with calcination temperature were studied to collect information on the state and stability of the additives in impregnated samples.

2. Experimental procedure

2.1. Sample preparation

Meta-stannic sol (parent sol) was precipitated from a cold solution of $SnCl_4$ (27%) by treating with an aqueous ammonia solution (28%), followed by thorough washing with deionized water. The sol was stocked in an air-tight plastic bucket as a source for the subsequent sample preparation. Pure powder of SnO_2 was obtained by drying the parent sol at 100 °C, followed by grinding to granules of 1–10 μm. The sample was actually hydrous SnO_2 which contained 13.8% water and consisted of primary particles of a few nanometres in size, as observed by electron microscopy.

For impregnation, the hydrous powder was mixed with an aqueous solution of a salt and/or polyoxy acid of the selected metal, M, or non-metal, A, element. The resulting suspension was then dried and ground. The amounts of M and A were fixed to 5% in atomic composition defined as M/(M + Sn) or A/(A + Sn) unless noted otherwise. The selected additives covered 31 metals (Li, Na, K, Rb, Cs, Mg, Ca, Ba, Sr, V, Cr, Mn, Fe, Co, Ni, Cu, Zn, Ga, Nb, Mo, In, La, Ce, Pr, Nd, Sm, Gd, W, Tl, Pb, and Bi) and 3 non-metals (S, B and P). As starting salts, metal acetates were used whenever available. The other salts used were nitrates (indium, gallium and bismuth), an oxalate (niobium), and polyoxy salts (NH_4VO_3, $(NH_4)_6Mo_7O_{24}$, $5(NH_4)_2 \cdot 12WO_3 \cdot 5H_2O$). The samples thus prepared were labelled M–SnO_2, A–SnO_2, or A–M–SnO_2, where the latter indicates double impregnation with A and M.

0022–2461

2.2. Physicochemical measurements

Specific surface area, SA, was evaluated from nitrogen adsorption data using the Brunauer, Emmett, Teller (BET) method. Each powder sample was cold-pressed at 200 kg cm^{-2}, crushed and sieved to 24–60 mesh granular, and outgassed at 300 °C for 1 h before nitrogen adsorption.

The mean crystallite size of SnO_2 was evaluated from X-ray diffraction (XRD) line (1 0 1) recorded on a Regaku 4011 diffractometer, based on Scherrer's equation. In some cases, the crystallite size was determined from the direct observation carried out on a transmission electron microscope (TEM; JEM 2000 EX). For TEM observation, the sample powder was sieved to granules under 235 mesh, and dispersed in methyl alcohol under supersonic vibration. A drop of the dilute suspension was taken on a collodion film, and soaked up with a filter paper.

The electrical resistance of pure and impregnated samples was investigated in the form of porously sintered elements. Each powder sample, calcined at 600 °C (impregnated SnO_2) or a specified temperature between 400 and 900 °C (pure SnO_2) for 1 h in air, was mixed with water. The resulting paste was applied to 1.0 mm thickness on an alumina tube with two platinum coil electrodes attached 1.5 mm apart from each other.

3. Results and discussion

3.1. Specific surface area

The thermal sintering of SnO_2 particles was investigated from the specific surface area, SA, after calcination at varying temperatures for 1 h. Fig. 1 shows the SA of some typical samples as a function of calcination temperature. Pure SnO_2 had an SA as large as 154 m^2 g^{-1} after calcination at 300 °C, but it decreased to 24 and 7 m^2 g^{-1} after calcination at 600 and 900 °C, respectively. On the other hand, all the impregnated samples retained larger SAs than the pure sample at 600 °C, indicating that the additives are more or less effective to increase the resistance to thermal sintering up to such a medium temperature. In the higher-temperature region, however, behaviour largely depended on the additives. That is, some additives such as phosphorus and barium were still effective in retaining a far larger SA than that of pure SnO_2 even at 900 °C while others, such as vanadium and sulphur, were not. Thus the additives can be classified into two types, i.e. one type which is effective in retarding the sintering of SnO_2 particles over the whole temperature range examined (Type I) and the other effective only up to a medium temperature (Type II).

The SA data for all the samples calcined at 600 and 900 °C for 1 h are listed in Table I. It is seen that Type II includes alkali metals, vanadium, sulphur,

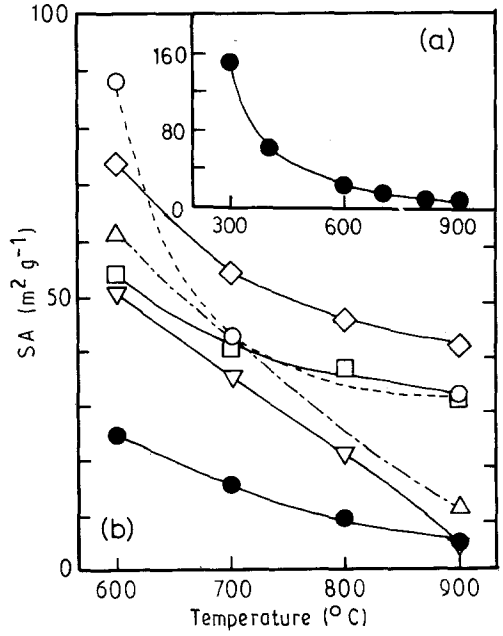

Figure 1 Specific surface area of some typical samples as a function of calcination temperature. Additives: (●) SnO_2, (○) P, (◇) P–V, (△) Cs, (□) Ba, (▽) V.

TABLE I Specific surface area and crystallite size after calcination at 600 and 900 °C

Additive 5 at %	600 °C		900 °C	
	SA (m^2 g^{-1})	D (nm)	SA (m^2 g^{-1})	D (nm)
none	24	13.8	6	27.2
Li	38	7.0	4	–
Na	44	10.0	5	–
K	54	9.2	5	33.0
Rb	55	7.8	–	–
Cs	62	9.0	12	26.2
Mg	52	5.2	22	12.5
Ca	40	5.2	20	9.5
Ba	54	5.7	33	8.6
Sr	58	5.1	23	9.9
V	51	6.7	6	38.2
Cr	41	7.1	–	9.9
Mn	37	6.1	24	14.0
Fe	39	7.2	20	18.2
Co	28	7.1	6	31.9
Ni	44	5.8	23	13.1
Cu	29	7.3	4	42.0
Zn	48	5.7	21	11.8
Ga	35	9.4	21	17.6
Nb	48	5.5	31	10.0
Mo	36	6.3	23	8.7
In	42	7.1	26	9.9
La	41	9.0	24	9.6
Ce	35	6.7	24	10.1
Pr	41	6.4	26	–
Nd	35	7.0	25	–
Sm	38	5.6	24	8.3
Gd	38	5.9	29	–
W	55	6.6	29	9.3
Tl	30	12.5	9	35.0
Pb	70	5.9	28	17.4
Bi	53	6.4	24	12.1
S	86	5.1	6	25.4
B	84	6.4	6	–
P	88	4.3	34	8.8
S–V	93	5.2	7	21.8
B–V	87	4.9	6	41.2
B–Ba	98	4.0	31	10.7
P–Ba	77	4.4	39	6.7
P–V	74	4.9	42	12.0

boron, copper, iron and thallium. On the other hand, Type I consists of alkaline earth metals, some transition metals, rare-earth metals and phosphorus, among which, phosphorus, barium, niobium, tungsten and gallium are especially effective up to 900 °C. The stabilizing effect became more pronounced in some cases where two additives were doubly impregnated: The samples with P–V and P–Ba showed the highest SA ($\sim 40\ m^2\ g^{-1}$) after calcination at 900 °C.

As seen from Table I, most non-metal additives (sulphur, boron and phosphorus) give particularly large SA exceeding $80\ m^2\ g^{-1}$ at 600 °C. These additives are expected to be strongly bonded to the SnO_2 surface as polyoxy cluster anions, giving rise to very marked effects up to the medium temperature (600 °C). The effects of sulphur and boron disappear at 900 °C, however, because of sublimation. A similar explanation may be possible for high valence metal additives such as vanadium, niobium and tungsten which also form polyoxy anions. The other additives having remarkable stabilizing effects at 600 °C were lead, caesium, strontium and barium, all of which have large ionic radii. Poorly mobile species seem to be effective for the stabilization.

So far the calcination time was fixed to 1 h. Fig. 2 shows the influence of calcination time at 900 °C on SA for typical samples. Although some samples tended to change gradually with time, the changes were rather slight over 12 h. It appears that SA is sensitive to calcination temperature but not so sensitive to calcination time. This stimulated evaluation of the stabilizing effect from the data after calcination for 1 h. The influence of the amounts of additives was also investigated for a few systems calcined at 600 °C. As shown in Fig. 3, P–SnO_2 was almost saturated in SA at 5 at % P, while Ba– and V–SnO_2 were still increasing in SA at 5 at %. The optimum amounts thus appear to be largely dependent on the additives used. Therefore, the data for 5 at % additives should be taken to just show the stabilizing tendency.

3.2. SnO_2 crystallite size

Fig. 4 shows XRD patterns of SnO_2, Ba–SnO_2 and Co–SnO_2 after calcination at 600 °C as well as 900 °C for 1 h. As an internal standard, 30 wt % silicon powder (particle size larger than 1 μm) was mixed with each sample. After calcination at 600 °C, diffraction peaks of SnO_2 were broad, especially in the impregnated samples, suggesting small sizes of the crystallites included. After calcination at 900 °C, the diffraction peaks remained broad for Ba–SnO_2, while they became sharp for Co–SnO_2, indicating that they belong to type I and II additives, respectively. In the case of

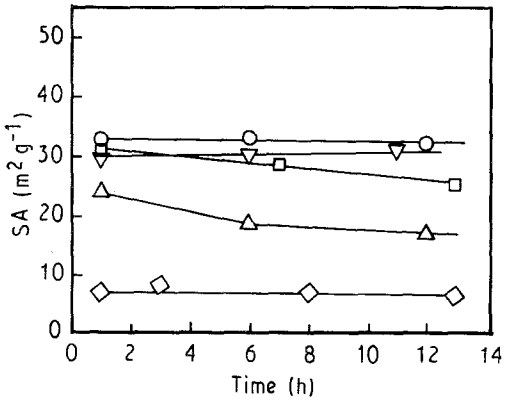

Figure 2 Influence of calcination time at 900 °C on specific surface area. (○) Nb, (▽) W, (□) Ba, (△) La, (◇) SnO_2.

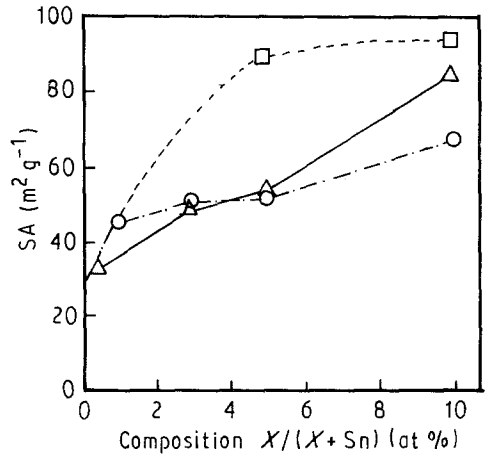

Figure 3 Influence of the amounts of additives (in atomic %) on specific surface area after calcination at 600 °C. (□) P, (△) Ba, (○) V.

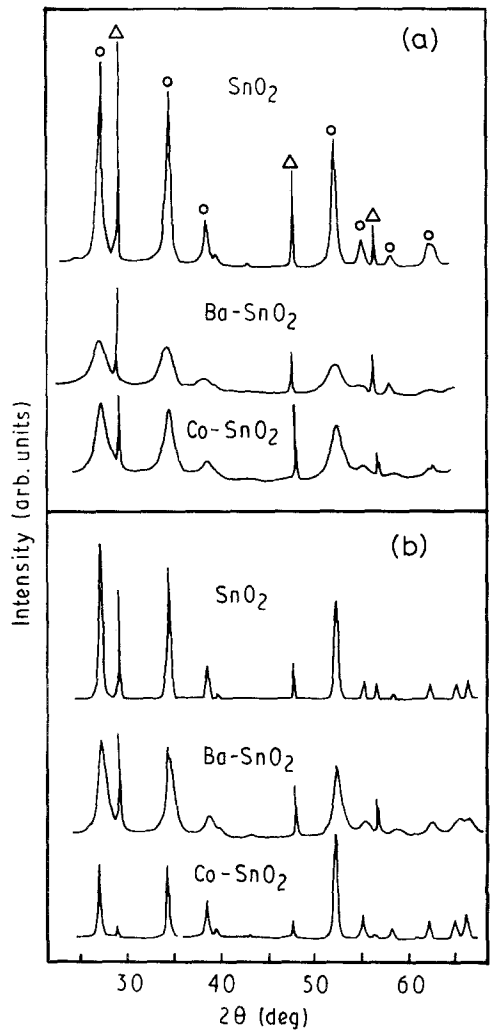

Figure 4 XRD patterns of SnO_2, Ba–SnO_2 and Co–SnO_2 after calcination at (a) 600 °C and (b) 900 °C for 1 h. (○) SnO_2, (△) Si.

Co–SnO_2, a small diffraction peak ascribable to CoO (2 2 0) was observed at $2\theta = 61.34°$, after calcination at 900 °C. Similar X-ray investigations were extended to all impregnated samples. In these diffraction patterns, the peak width changed variously, but no significant changes were detected in the diffraction angles. It follows that most of the additives do not enter the SnO_2 lattice in the bulk significantly during the heat treatment applied.

The mean size, D, of SnO_2 crystallites was evaluated from the width of the (1 0 1) diffraction peak. Fig. 5 shows the D values as a function of calcination temperature for some selected samples. In pure SnO_2, D increased monotonically from 4 nm at 400 °C to 27.2 nm at 900 °C. In most of the impregnated samples, on the other hand, D remained at a much smaller size, although some additives, such as cobalt, promoted the grain growth of SnO_2. The D data for all the samples after calcination at 600 and 900 °C are listed in Table I along with the SA data. These data show that D can be controlled to a size from 4–42 nm by properly choosing the additives and calcination temperature.

Based on the D data, the stabilizing effects of additives during calcination at 900 °C can be classified into four groups as follows.

Group A: very marked effect ($D < 10$ nm)
P–Ba, Sm, Ba, P, Mo, W, Ca, Sr, Cr, In
Group B: marked effect ($10 \text{ nm} \leqslant D < 13$ nm)
Nb, Ce, Pr, Nd, Gd, B–Ba, La, Zn, P–V, Bi, Mg
Group C: noticeable effect ($13 \text{ nm} \leqslant D < 18$ nm)
Ni, Mn, Pb, Ga
Group D: little or no effect ($18 \text{ nm} \leqslant D$)
Fe, S–V, S, B, Li, Na, Cs, Co, K, Tl, V, B–V, Cu.

Groups A, B and C belong to Type I and Group D to Type II, according to the previous classification.

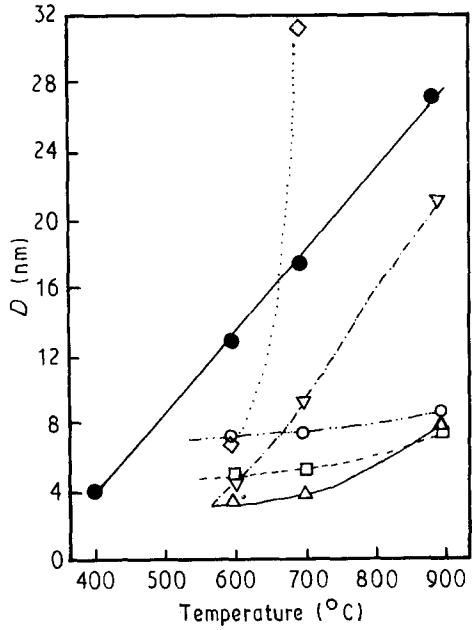

Figure 5 Crystallite size of SnO_2 as a function of calcination temperature for some selected samples. (●) SnO_2, (◇) Co, (▽) S, (○) La, (□) Ba, (△) P.

Some Group D additives (K, V, Co, Cu, Tl, B–V) give larger D values than the pure samples after calcination at 900 °C, suggesting that they rather promote the grain growth of SnO_2.

3.3. Electron microscopic observation

In order to collect further information on the crystalline state, some calcined samples were subjected to direct observation by transmission electron microscopy (TEM). Fig. 6 shows TEM images of crystallites for pure SnO_2, Ca–SnO_2 (Type I), and Co–SnO_2 (Type II). In the pure sample, calcination at 400 °C (a) gave SnO_2 particles of about 4 nm diameter, which were heavily aggregated together. The particles became more and more coarse on increasing the calcination temperature to 700 °C (b) and 900 °C (c). For Ca–SnO_2, ultrafine particles were seen after calcination at both 600 °C (d) and 900 °C (e), while Co–SnO_2 gave ultrafine particles at 600 °C (f) but very coarse particles at 900 °C (g).

The sizes of more than 200 SnO_2 particles were measured on such TEM images for each sample. The resulting particle size distributions for two examples of pure SnO_2 and Ca–SnO_2 are shown in Fig. 7. It is noted that the dispersion of particle size is rather narrow, and Ca–SnO_2 contains ultrafine particles around 10 nm even after calcination at 900 °C. From these particle size distributions, mean particle sizes were evaluated and compared with the crystallite sizes, D, evaluated from X-ray diffraction. As shown in Table II, both values are seen to coincide well with each other. This indicates that the particles observed in the TEM images are in fact the crystallites of SnO_2, or, in other words, there is little possibility of the inclusion of amorphous phases.

As shown from previous TEM images, each SnO_2 crystallite was mostly connected with its neighbours by necks. The relation between neck size in diameter, X, and crystallite size, D, was investigated by measuring them on TEM images, because these parameters have significant meaning in gas sensors. Fig. 8 shows the data of X and D for pure and some impregnated samples. Clearly X is fairly proportional to D, with a proportionality constant, $k = X/D$, being equal to 0.80 ± 0.10, in common for both pure and impregnated samples.

3.4. Coagulation structure of SnO_2 crystallites

It is interesting to compare D with SA quantitatively. Fig. 9 plots the relation between D and SA for all the investigated samples. When all particles are free, D and SA are correlated by $SA = K/\rho D$, where ρ is the specific density of particles (7.0 g cm^{-3} for SnO_2), and K is a shape factor [7]. A theoretical relation for free spherical particles ($K = 6$) is shown by a solid line in the figure. Obviously, observed SA data all scatter below this correlation line, lying between 23% and 58% of the theoretical values of free spheres. These discrepancies are not surprising, because actual particles are coagulated together by forming necks and

grain boundaries. These SA data rather suggest that each SnO_2 crystallite has a considerable portion of free surface to be exposed to the surrounding atmosphere. It has been reported that SnO_2 samples have no closed pores even when calcined at 1200 °C [8–10].

As revealed from the above TEM observation, crystallites in each sample have a rather uniform size, D, and are connected with neighbours by necks of a size, X, proportional to D. On such backgrounds, it is reasonable to consider that the deviation of observed SA from the free sphere model can be ascribed to the loss of free surface of each crystallite due to neck formation. It is assumed that the powder consists of uniform crystallites and each crystallite is a spherical particle except those parts deleted for neck formation. When each crystallite is coordinated with N neighbours (coordination number N), and $X/D = k$, simple geometrical derivation leads to the following expression for specific surface area, SA

$$SA = \frac{6}{eD} F(k, N) \quad (1)$$

$$F(k,N) = \frac{4 - 2N[1 - (1 - k^2)^{1/2}]}{4 - N[1 - (1 - k^2)^{1/2}]^2[2 + (1 - k^2)^{1/2}]} \quad (2)$$

$F(k,N)$ is a microstructure factor related to N and k. If $N = 0$ or $k = 1$, $F(k,N) = 1$, then this model is

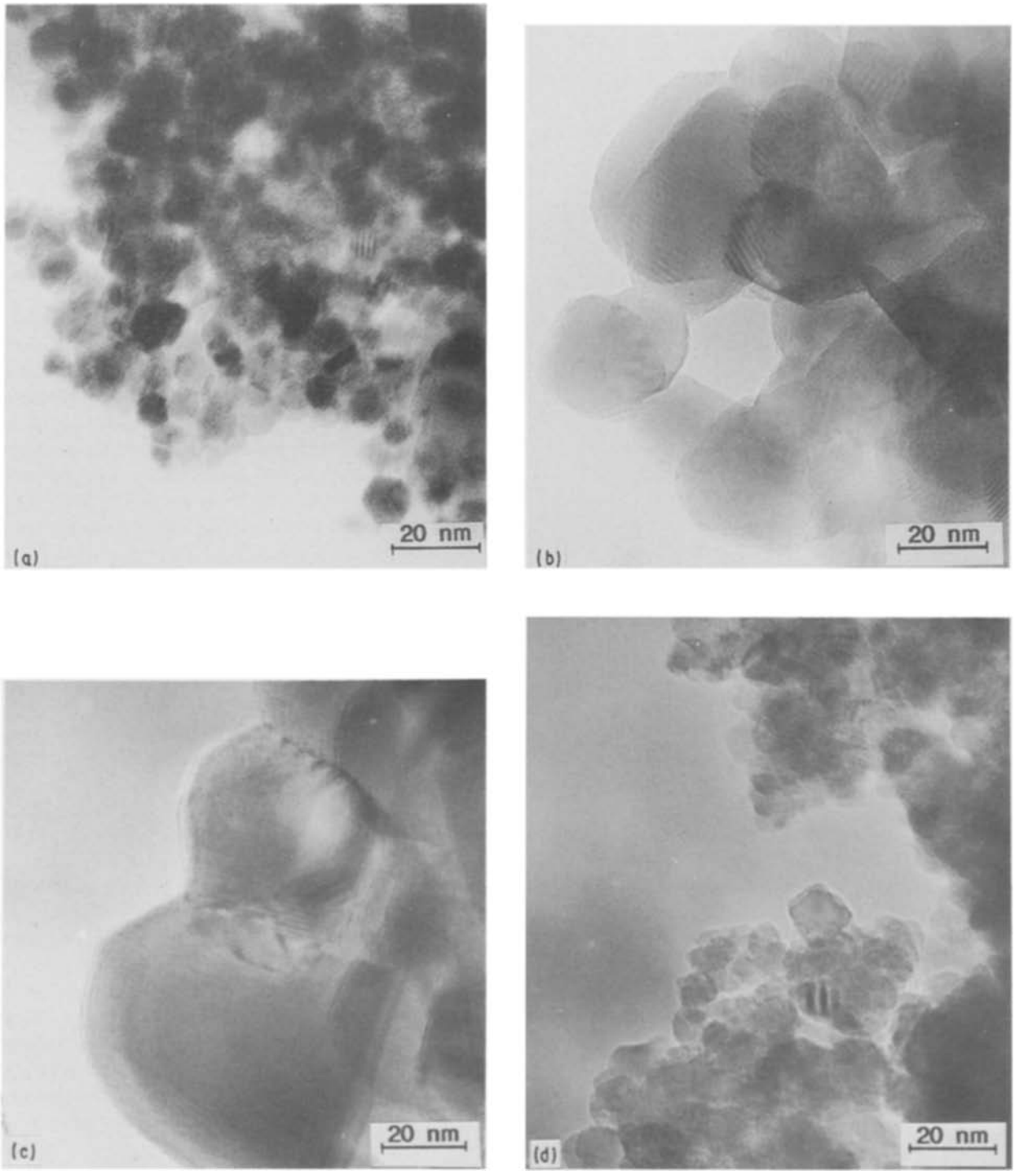

*Figure 6*a–d TEM images of (a–c) pure SnO_2, (d, e) Ca–SnO_2 and (f, g) Co–SnO_2 after calcination at (a) 400 °C, (b) 700 °C, (c) 900 °C, (d) 600 °C, (e) 900 °C, (f) 600 °C, (g) 900 °C for 1 h.

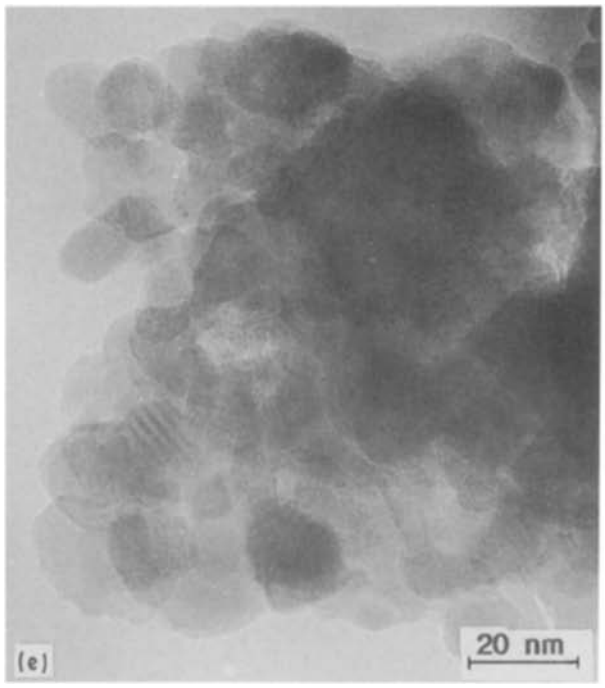

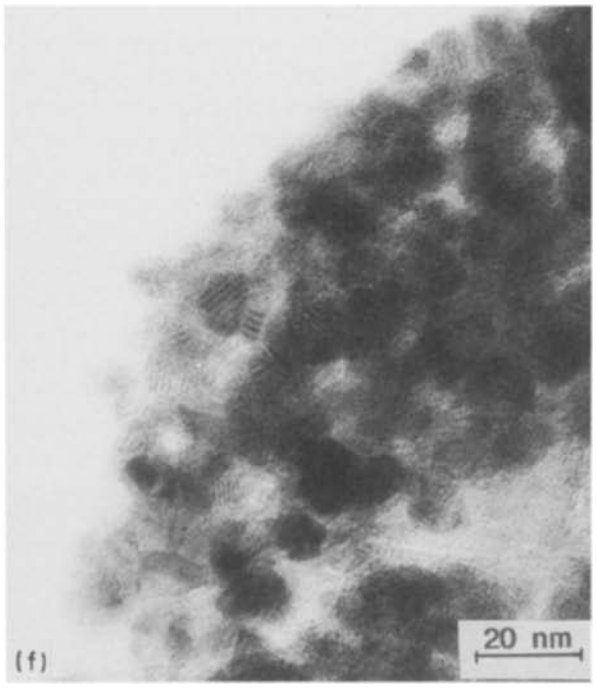

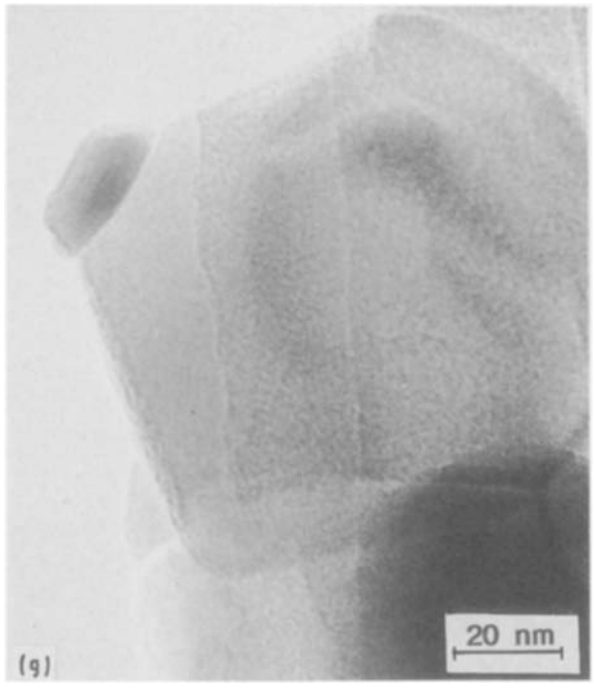

Figure 6 Continued.

reduced to the free sphere model. When $k = 0.80$ for the samples investigated as mentioned above, SA is thus dependent on N. Theoretical relations between SA and D based on this coagulation model are indicated by straight lines for $N = 3$, 4 and 4.5 in Fig. 9. Experimental data are seen to scatter between $N = 3$ and 4.5, and most frequently around $N = 4$. In this way, the crystallites of SnO_2 in most samples can be pictured as being coordinated with four neighbouring particles on average.

3.5. Electrical resistance

The electrical resistance was measured by using sintered elements fabricated with the prepared powder samples. Fig. 10 shows the electrical resistance measured at 300 °C in air for various impregnated systems as well as pure SnO_2 systems, as a function of SnO_2 crystallite size, D. In this case, the impregnated systems had been sintered (calcined) in the form of elements at 700 °C, and the elements were destroyed afterwards to determine D values from X-ray diffraction analyses. For the pure system, SnO_2 powder calcined at a temperature in the range 400–900 °C was used to fabricate elements, which were then sintered at 400 °C.

As seen from Fig. 10, electrical resistance, R, is strongly dependent on D even for the pure SnO_2 system. It was previously reported [1] that this dependency is related to the surface space charge formed on each semiconducting particle. Because the depth of the surface space charge, L, of pure SnO_2 is about 3 nm, R increases steeply as D decreases in the region $D < 2L$, while R is far less dependent on D in the larger D region.

The electrical resistance of the additive-impregnated elements is never simple, because not only is it susceptible to such a grain size effect but also it is influenced by the properties and existing state of the additives. Generally speaking, however, R values for most impregnated systems tend to scatter in the region somewhat above the correlation line of the pure SnO_2 system. This seems to suggest that most additives do not affect the electrical properties of SnO_2 particles so much under these conditions, although they increase the resistance of the elements to some extent. Exceptionally high or low resistance was observed with cobalt, iron, magnesium and boron as indicated in the figure.

In conjunction with the stabilizing effects of additives in the high-temperature region, the electrical resistance of each element (measured at 500 °C) was

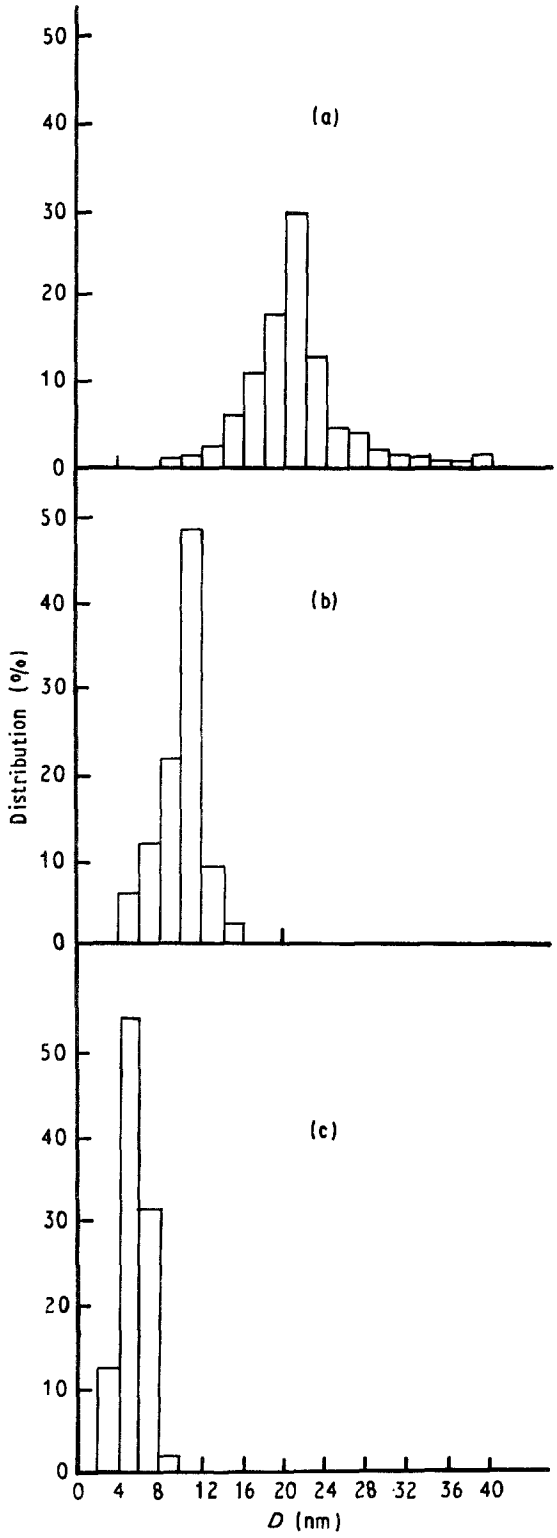

Figure 7 Particle size distribution for (a) pure SnO_2 and (b, c) Ca–SnO_2, calcined at (a) 700 °C, (b) 900 °C, (c) 600 °C for 1 h.

TABLE II Comparison of mean particle size evaluated from TEM and XRD

Sample	Calcination[a]		Crystallite size (nm)	
	(°C)	(h)	XRD	TEM
SnO_2	400	1 h	4.8	5.0
SnO_2	700	1 h	18.2	20.6
SnO_2	900	1 h	27.2	31.8
Ca–SnO_2	600	1 h	5.2	5.8
Ca–SnO_2	900	1 h	9.5	10.0

[a] Temperatures and duration of calcination.

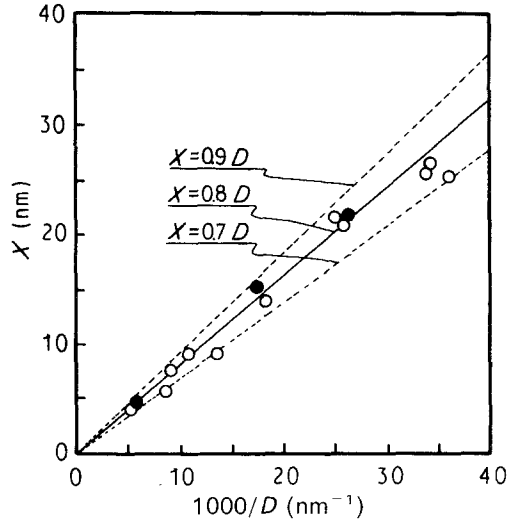

Figure 8 Relation between neck size, X, and crystallite size, D, for (○) pure SnO_2 and (●) impregnated samples.

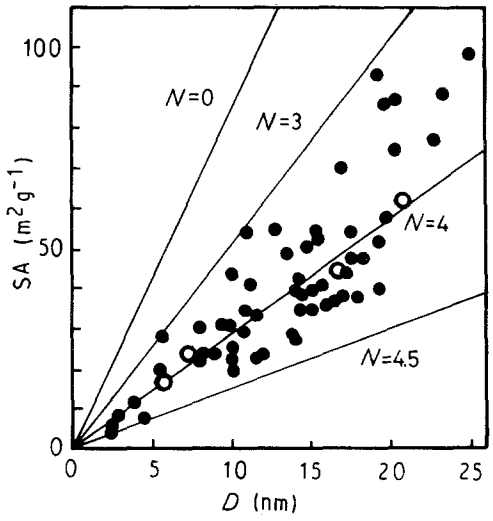

Figure 9 Relation between crystallite size, D, and specific surface area, SA, for (○) pure SnO_2 and (●) impregnated samples. (——) Theoretical relations based on a monolised sphere model for coordination number $N=0$, 3, 4 and 4.5.

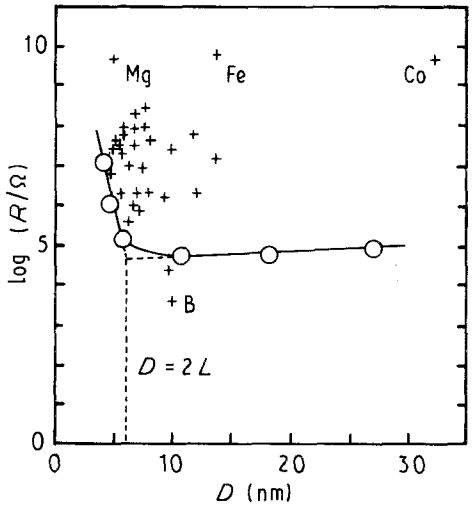

Figure 10 Electrical resistance, R, at 300 °C in air for (○) pure SnO_2 elements sintered at 400 °C and (+) various impregnated elements sintered at 700 °C, as a function of SnO_2 crystallite size, D. L is the depth of space charge layer of pure SnO_2 (~3 nm).

investigated by increasing the sintering temperature, T_s, stepwise from 600 °C to 900 °C at intervals of 100 °C. For simplicity, the electrical resistance was normalized at the value after calcination at 600 °C, $R(600)$, and the relative value, $\delta = R(T_s)/R(600)$, was used for this purpose. Fig. 11 shows log δ as a function of T_s. The pure element showed increased δ gradually with increasing T_s. Impregnated elements, however, behaved very differently, depending on the additives. Three types of δ–T_s behaviour were recognized, i.e. (a) monotonic increase, (b) decrease followed by increase, and (c) monotonic decrease of δ with increasing T_s. Typical additives giving rise to the respective types are as follows:

Type a: Bi, La, Pb, Zn
Type b: V, B, P, Ca, P–V
Type c: Nb, W, Ba.

It is noted that Type II additives (such as boron and vanadium) tend to give Type b behaviour. This probably reflects that the additives disappear from the surface of SnO_2 in the temperature range studied. δ–T_s behaviour, however, is very complicated. It can be affected by any changes in microstructure of the elements, such as grain growth of SnO_2, segregation or disappearance of additives, and the formation of new compounds or solid solution between additives and SnO_2. Further studies based on these respects are necessary to account for δ–T_s behaviour.

3.6. Stabilizing mechanism of additives

Tin oxide is known as a typical oxide following a thermal sintering mode where grain growth takes place without a change in porosity (or apparent density) [11, 12]. Such a mode is possible when the grain growth proceeds through a surface diffusion mechanism or evaporation–condensation mechanism [13].

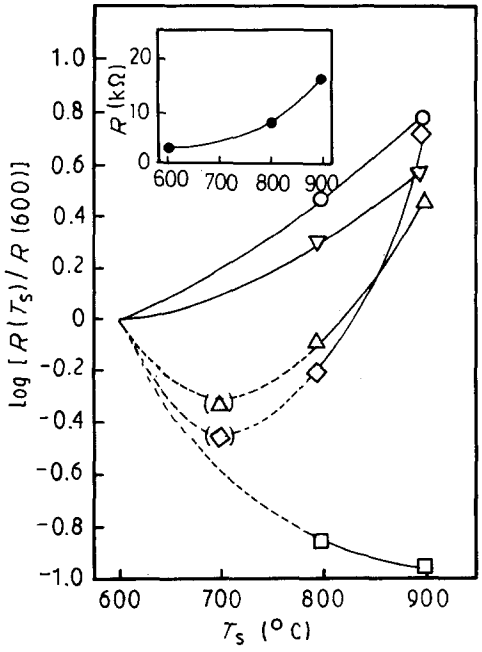

Figure 11 Relative electrical resistance as a function of sintering temperature. (Resistance measured at 500 °C.) (○, ●) SnO_2, (▽) P–V, (△) V, (◇) B, (□) Nb.

It has been reported that the former and latter mechanisms operate in the grain growth of SnO_2 at lower and higher temperature regions, respectively [14, 15]. The stabilizing effects of additives on the grain growth of SnO_2 in this study (below 900 °C) appear to be related to the ability to suppress the surface diffusion mechanism.

It was shown that all the additives were effective more or less up to the medium temperature of 600 °C. Type II additives, consisting of alkali metals, vanadium, copper, cobalt, sulphur and boron, lose their effects at higher temperature; as these additives are subject to segregation, melting or sublimation at 700–900 °C, their disappearance from the surface of SnO_2 crystallites seems to be the main cause of the losses of stabilizing effects. In the case of Co– and Cu–SnO_2, the formation of CoO and CuO was detected by XRD after calcination at 900 °C. In the case of V–SnO_2 calcined at 800 °C, some of the vanadium ions were confirmed to form a solid solution with SnO_2 by means of XRD analysis.

On the other hand, Type I dopants appear to stay more firmly on the surface of SnO_2 crystallites. XRD analyses showed that after calcination at 600 °C, there were no crystalline phases other than SnO_2 itself in all the 5 at % impregnated samples examined, except Cr–SnO_2 for which a free oxide of Cr_2O_3 was detected. For other impregnated systems, free compounds of additives were detected at far larger loadings. In the cases of V– and Ba–SnO_2 systems, for example, V_2O_5 and $BaCO_3$ were detected at 20 at %, respectively, while Mo–SnO_2 showed no additive compound up to 40 at %. It seems that most additives are well dispersed on the surface of SnO_2 ultrafine particles. It can be shown that, when SnO_2 has specific surface area of 200, 100, 50 and 25 $m^2 g^{-1}$, a monolayer coverage on it requires 37%, 19%, 10% and 5% loadings, respectively. Thus the loadings level of 5 at % is, in many cases, below a monolayer coverage for most of the Type I additives. It is suggested that additives dispersed well on the surface of SnO_2 provide a barrier for surface diffusion thus suppressing crystal growth or coagulation of SnO_2 particles during calcination. It seems that the more stable the additives on the SnO_2 surface are, the more effectively the ultrafine particles of SnO_2 could be stabilized.

4. Conclusions

1. Specific surface area, SA, data revealed distinction between additives which were effective to stabilize ultra fine particles of SnO_2 up to 900 °C (Type I) and those effective only up to 600 °C (Type II).

2. XRD data on SnO_2 crystallite size, D, showed the variation of stabilizing effects with additives more clearly. The most effective additives (Group A) could stabilize SnO_2 crystallites at less than 10 nm in size, even after calcination at 900 °C.

3. TEM observation indicated that the dispersion of crystallite size was rather narrow and that the mean crystallite sizes based on TEM coincided well with D values based on XRD.

4. TEM observation also revealed a relation between neck size, X, and crystallite size, D: X was fairly proportional to D with a proportionality constant (X/D) of 0.80 ± 0.10, throughout the samples investigated.

5. Analysis of SA and D data based on a monosized sphere model suggested such a coagulation structure that each SnO_2 crystallite is coordinated with 3–4.5 neighbours through necks of a size X.

6. Electrical resistance, R, of impregnated samples scattered in most cases somewhat above the correlation line between R and D for pure SnO_2 samples, suggesting that most additives do not affect significantly the electrical properties of SnO_2 particles.

7. It is proposed that additives, when dispersed and immobilized on the surface of SnO_2 crystallites, retard surface diffusion which leads to the grain growth of SnO_2.

References

1. C. XU, T. TAMAKI, N. MIURA and N. YAMAZOE, *J. Electrochem. Soc. Jpn* **58** (1990) 1143.
2. H. OGAWA, A. ABE, M. NISHIKAWA and S. KAYAKAWA, *J. Electrochem. Soc.* **128** (1981) 695.
3. T. SUZUKI, T. YAMAZAKI and K. TAKAHASHI, *J. Mater. Sci. Lett.* **24** (1989) 2127.
4. S. TANG, M. YUAN, D. XU and Z. LAI, in Digest of Technical Papers of Transducers '87, Tokyo (1987) p. 631.
5. M. J. FULLER, M. E. WARWICK and A. WALTON, *J. Appl. Chem. Biotechnol.* **26** (1976) 396.
6. C. XU, T. TAMAKI, N. MIURA and N. YAMAZOE, *J. Mater. Sci. Lett.* **8** (1989) 1092.
7. K. S. W. SING, in "Characterization of Powder Surface", edited by G. D. Parfitt and K. S. W. Sing (Academic Press, London, 1976) p. 1.
8. T. KIMURA, S. INADA and T. YAMAUCHI, *J. Mater. Sci.* **24** (1989) 220.
9. O. J. WHITTEMORE and J. A. VARELA, *Mater. Sci. Res.* **13** (1980) 51.
10. M. J. FULLER, *J. Appl. Chem. Biotechnol.* **28** (1978) 539.
11. K. IHOKURA, *Denki Kagaku* **50** (1982) 99.
12. T. QUADIR and D. W. RENDY, *Mater. Sci. Res.* **16** (1984) 159.
13. S. A. SELIM and F. I. ZEIDAN, *J. Appl. Chem. Biotechnol.* **26** (1976) 23.
14. S. J. PARK, K. HIRATA and H. YAMAMURA, *Ceram. Int.* **10** (1984) 116.
15. Z. A. MUNIR, P. K. HIGGINS and R. M. GERMAN, in "Sintering – New Developments", edited by M. M. Ristic (Elsevier, 1979) p. 26.

Received 15 October 1990
and accepted 25 March 1991